The Effects of CISD2 Knockout on Mitochondrial Morphological Subtypes in 3D Micrographs of Mouse Epidermal Tissues

Jia-Mei Lu, Chung-Chih Lin, Kuan-Sheng Wu, Ting-Fen Tsai, Jyh-Ying Peng, Han-Wei Dan, and Yuh-Show Tsai

Abstract

CISD2, CDGSH Iron Sulfur Domain 2, is a gene associated with Wolfram Syndrome. Lack of CISD2 results in premature aging. Such defects can cause skin thinning and activate mitophagy and mitochondrial disorder. However, the effects of CISD2 knockout on mitochondrial dynamics of skin tissues are unclear because lack of 3D mitochondrial morphological analysis in tissues. In this paper, 3D micrographs of mouse epidermal tissue in normal and premature aging (CISD2 knockout) mice expressing Dendra2-mito, which visualized mitochondrial morphology, were analyzed. Cells at different depths of skin layers were analyzed separately. Mitochondrial objects were segmented by MicroP, and then used for acquiring 3D morphological features. Features have been normalized to cluster mitochondrial objects into mitochondrial subtypes by X-means. There were total 7 mitochondrial morphological subtypes in epidermal tissue, and the distributions of each subtype between normal and premature ageing epidermal cells were different.

Keywords

Mitochondrial morphology • CISD2 • Numerical 3D image analysis

1 Introduction

Mitochondria play an important role in many cellular functions, including supplying energy, signaling, differentiation, and apoptosis. CISD2, CDGSH Iron Sulfur domain 2, is one of mitochondrial outer membrane proteins and associated with Wolfram syndrome (WFS). WFS is a recessive genetic disease that may induce diabetes, optic atrophy, and deafness. Recent studies showed that lack of CISD2 could cause mitochondrial dysfunctions to induce mitophagy (selective autophagy of mitochondria) and result in premature aging disorder [1, 2]. Mitochondrial dynamics is highly correlated with mitochondrial functions and dysfunctions. But the effects of CISD2 knockout on mitochondrial dynamics of skin tissue are unclear. Mitochondrial dynamics includes fission, fusion, trafficking, biogenesis, and mitophagy. All the functions of regulatory proteins involved in mitochondrial dynamics can affect morphology and distribution of mitochondria in cells [3]. By 3D mitochondrial morphological analysis in tissues, researchers can learn more about the relationship between mitochondrial morphologies and premature aging in skin tissues. Accomplished results will evaluate whether 3D skin mitochondrial dynamics is a potential biomarker for diagnosis of premature ageing.

In this study, the subtypes of 3D mitochondrial morphologies were clustered to identify the effects of CISD2-knockout on mitochondrial morphology of mouse epidermal tissues at different depth.

J.-M. Lu · H.-W. Dan · Y.-S. Tsai (✉)
Department of Biomedical Engineering and Center of Biomedical Technology, Chung Yuan Christian University, 200 Chung Pei Road, Taoyuan, Taiwan
e-mail: yuhshow@cycu.edu.tw

C.-C. Lin · K.-S. Wu · T.-F. Tsai
Department of Life Sciences and Institute of Genome Sciences, National Yang-Ming University, Taipei, Taiwan

J.-Y. Peng
Department of Data Science Team, Vpon Inc, Taipei, Taiwan

T. Vo Van et al. (eds.), *6th International Conference on the Development of Biomedical Engineering in Vietnam (BME6)*, IFMBE Proceedings 63, https://doi.org/10.1007/978-981-10-4361-1_15

2 Materials and methods

2.1 Images

The 3D microscopic images of mitochondria in skin tissues of CISD2 knockout (CISD2-KO) and Wild type (WT) mice expressing Dendra2-mito were acquired by intravital laser scanning confocal microscopy. The single-cell image stack sets and numbers are listed in Table 1. Layer 1 and 2 represent different depths of skin tissues, which layer 1 contains surface layers and layer 2 contains deeper layers of skin tissues.

2.2 Procedures for Subtypes Identification

Figure 1 shows the design of flowchart for finding 3D morphological subtypes of mitochondria. Slices of single-cell image stacks were applied to the following process. First, MicroP was used for segmenting mitochondrial objects. Binary images of stacks were applied to ImageJ plugin for extracting 3D morphological features. Morphological features were applied to X-means for clustering mitochondrial morphological subtypes. The ratios of every cluster in cells would be calculated. The detailed explanations will be described in the following sections.

2.3 Segmentation of Mitochondria

MicroP [4] was a tool developed under MATLAB, which could automatically segment mitochondrial objects in 2D images. For optimal mitochondrial segmentation, users could modify the parameters manually. The basic algorithm of MicroP was Adaptive Local Thresholding (ALT). ALT used local mean (μ_s) and standard deviation (σ_s) for normalization in a defined region, and combined with double threshold T_0 and T_1. When pixel intensity was higher than T_0, treated as foreground; on the other hand, pixel intensity lower than T_1 was background. The processing of segmentation was shown in equation (1) [5], where t(x) was image pixel value, $p(x)$ was the processed value, and k was constant. The representative result of mitochondrial segmentation by MicroP is shown in Fig. 2.

$$\mathrm{t(x)} = \begin{cases} p(x) - T_0 & \text{if } p(x) \le T_0 \\ p(x) - T_1 & \text{if } p(x) \ge T_1 \\ p(x) - \mu_{s(x)-k\cdot\sigma_{s(x)}} & \text{if } T_0 < p(x) < T_1 \end{cases} \quad (1)$$

Table 1 Image types and numbers

Cell type	3D stack number
CISD2-KO layer1	4
CISD2-KO layer2	24
Wild type layer1	6
Wild type layer2	24

2.4 Acquisition of Morphological Features

There were three ImageJ plugins used for extracting 3D mitochondrial morphological features, including 3D Object counter [6], AnalyzeSkeleton (2D/3D) [7], and 3D Analysis (3D Shape measurements) [8]. There are total 15 features for clustering morphological subtypes, as shown in Table 2.

3D Object Counter could count the number of 3D objects, and quantify geometrics parameters such as volume, surface are, and solidity. This plugin could also find out the smallest box encompassing the objects, and calculate the width, height, depth, and the ratios pairwisely.

AnalyzeSkeleton (2D/3D) was applicable for analyzing the skeleton parameters of 2D or 3D images, and understanding the structure by branches length of objects. The features included branch number and branch length relevant parameters.

3D Analysis contained many different 3D analysis methods. The part used in this paper was shape measurements. It would calculate compactness, sphericity, and elongation of segmented objects.

2.5 Mitochondrial Morphological Subtypes Clustering

Unsupervised clustering method was always used to find the group structure of unlabeled data At the situation of not knowing how many subtypes of 3D mitochondrial morphologies, an efficient clustering method was necessary.

The most common non-hierarchical algorithm for clustering was K-means. Group number needed to be set in K-means. As long as the subtype number for this study was uncertain at the beginning, an extension method of K-means, X-means [9], was applied. In X-means, user was only asked to set a range of group number. The algorithm of comparison between data for clustering was based on Bayesian Information Criterion, as (2).

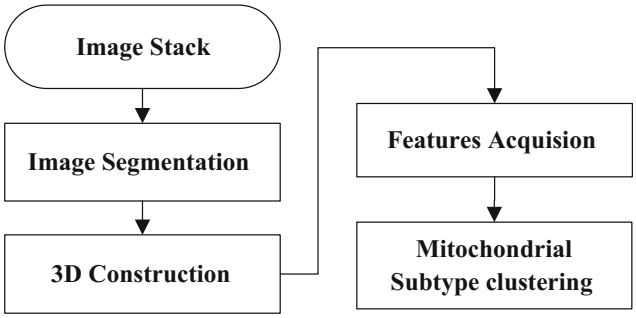

Fig. 1 Flowchart for identifying mitochondrial morphological subtypes

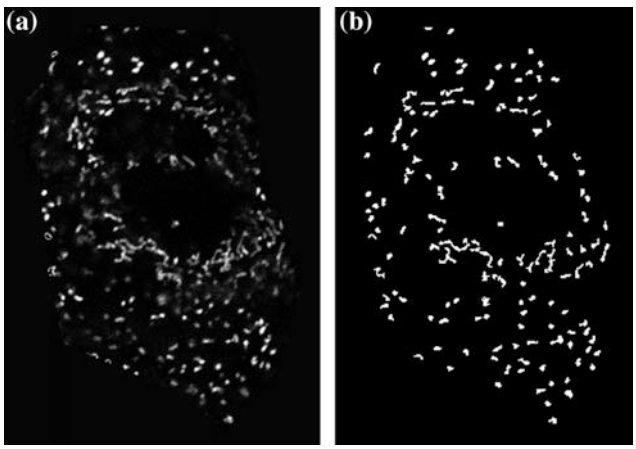

Fig. 2 Images of CISD2-KO at Layer 1, **a** is at the gray scale level, and **b** is the binary image

$\widehat{l}_j(D)$ point with the biggest possibility, p_j is data in M_j, and D is data point. (3) can lead to the result of $\widehat{l}_j(D)$.

$$\mathrm{BIC}(M_j) = \widehat{l}_j(D) - \frac{p_j}{2} \cdot \log D \tag{2}$$

$$\widehat{l}_j(D) = -\frac{D_n}{2}\log(2\pi) - \frac{D_n \cdot M}{2}\log(\sigma^2) - \frac{D_n - K}{2} + D_n \log D_n - D_n \log D \tag{3}$$

3 Results

3.1 Mitochondrial Morphological Subtypes

There were 7 morphological subtypes in mitochondria of skin cells. In Fig. 3, there are 15 typical objects showing in each subtype. The 15 objects were closest to mean position of X-means in every subtypes. Based on the morphological appearances, group A was like globule, and was the smallest dots. Group B and D were bigger with rougher surface, so called as small lump and big lump. Mitochondrial volume of group C was similar to those of groups B and D, but more elongated and named as short tubules. Group E, F and G were the most complicate structure with long branches and largest volume, so could be named as short, medium, and long branch types respectively. Figure 4 is a PCA plot to show that these 7 types are nicely separated.

Table 2 Mitochondrial morphological feature of 3D images

Feature name	Descriptions
Volume	Number of object's voxels
Surface area	Number of surface voxels
Solidity	Ratio of volume to surface area
Box width	Width of the smallest box encompassing the object
Box height	Height of the smallest box encompassing the object
Box depth	Depth of the smallest box encompassing the object
Axial ratio 1	Ratio of largest axis to minimum axis of the smallest box encompassing the object
Axial ratio 2	Ratio of second large axis to minimum axis of the smallest box encompassing the object
Branch	Number of skeleton branch
Total branch length	Total length of branches
Average branch length	Total length of branches per branch number
Maximum branch length	Length of the longest branch
Compactness	Normalized solidity
Sphericity	Cube root of compactness
Elongation	3D ellipsoid fitted to the object

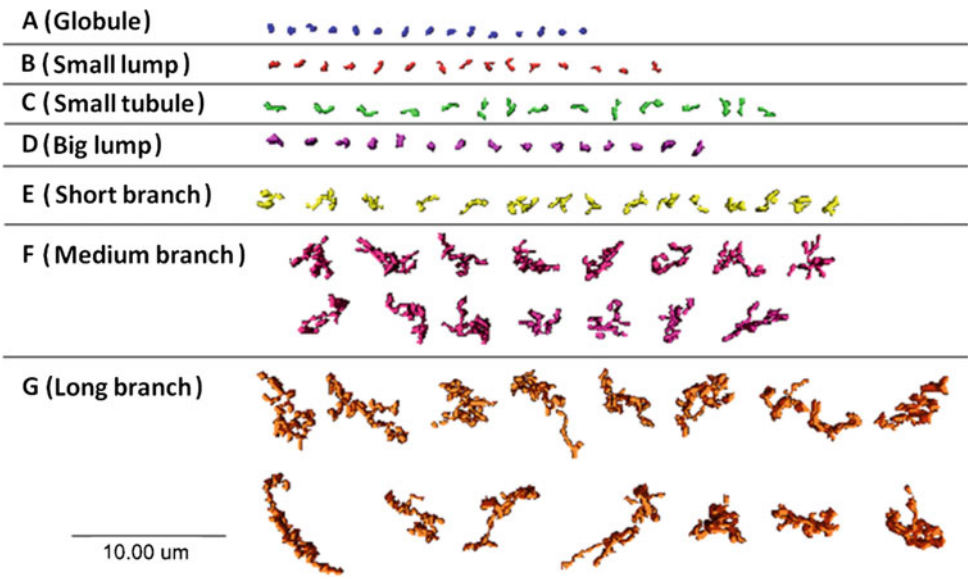

Fig. 3 3D mitochondrial morphological subtypes

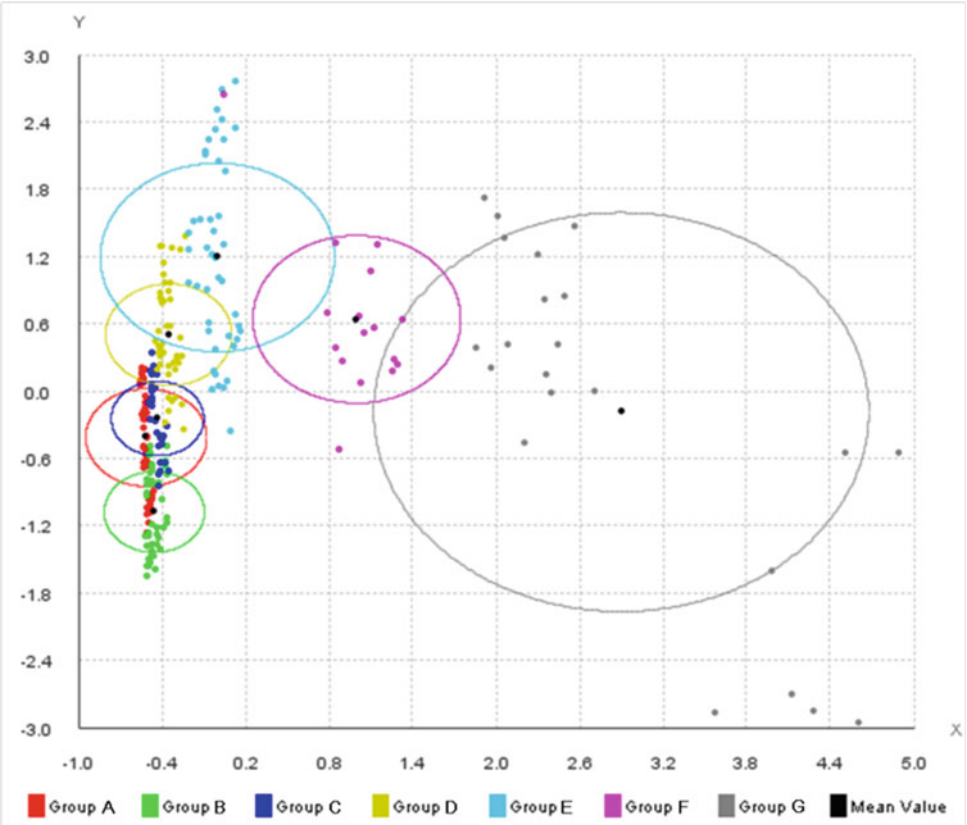

Fig. 4 Visualization of distances around 7 subtypes (by PCA)

Table 3 Ratio of subtypes in different cell types

	Globule (%)	Small lump (%)	Short tubule (%)	Big lump (%)	Short branch (%)	Median branch (%)	Long branch (%)
CISD2 -KO layer1	26.59	26.00	11.11	13.48	21.26	1.41	0.15
CISD2 -KO layer2	27.14	23.76	9.35	10.70	22.52	4.50	2.03
WT layer1	31.51	11.46	4.38	32.18	19.63	0.76	0.08
WT layer2	24.58	21.22	6.54	16.78	22.99	4.53	3.36

3.2 Subtype Composition of Cells

The ratios of objects number in each mitochondrial morphological subtype in individual cells were calculated, as equation (4), and the results are shown in Table 3.

$$\text{Ratio}\,(\text{X}) = \frac{\text{Number of mitochondrial objects in subtype}\,(\text{X})}{\text{Number of mitochondrial objects in whole cell}} \quad (4)$$

Comparing mitochondria in layer 1, there were more globule and big lump in normal cells (WT: 31 and 32%; CISD2-KO: 26 and 13%). On the other hand, there are more small lump and short tubule in premature aging cells (WT: 11 and 4%; CISD2-KO: 26 and 11%). In layer2, normal cells have more big lumps and less short tubules (WT: 16 and 6%; CISD2-KO: 10 and 9%).

4 Conclusion

According to 3D mitochondrial morphological features, there were 7 subtypes clustered based on 3D mitochondrial morphological features which were identified by X-means, including globule, small lump, big lump, short tubule, short branch, medium branch, and long branch. Based on the ratios of different subtypes of skin cells, there were different subtype distributions between the normal and premature aging mouse epidermal cells. In the future, we will increase mice and cell number to confirm results of this study. Moreover, we will include mouse at different age to identify the biomarker of ageing for screening drugs of rejuvenation.

References

1. Chen YF, Kao CH, Chen YT, Wang CH, Wu CY, Tsai CY, Liu FC, Yang CW, Wei YH, Hsu MT, Tsai SF, Tsai TF (2009) Cisd2 deficiency drives premature aging and causes mitochondria-mediated defects in mice. Genes Dev 23:1183
2. Wang CH, Chen YF, Wu CY, Wu PC, Huang YL, Kao CH, Lin CH, Kao LS, Tsai TF, Wei YH (2014) Cisd2 modulates the differentiation and functioning of adipocytes by regulating intracellular Ca2+ homeostasis. Human molecular genetics 23:4770–4785
3. Smirnova E, Shurland D, Ryazantsev SN, van der Bliek AM (1998) A human dynamin-related protein controls the distribution of mitochondria. J Cell Biol 143(2):351–358
4. Peng J-Y, Hsu C-N (2009) Adaptive Local Tresholding for fluorescence Cell Micrographs. Institute of Information Science, Academia Sinica, Taipei, Taiwan, ROC
5. Yan F, Zhang H, Kube CR, Yan F, Zhang H, Kube CR (2005) A multistage adaptive thresholding method. Pattern Recogn Lett 26:1183
6. Bolte S, CordeliÈRes FP (2006) A guided tour into subcellular colocalization analysis in light microscopy. J Microsc 224:213–232
7. Arganda-Carreras I, Fernández-González R, Muñoz-Barrutia A, Ortiz-De-Solorzano C (2010) 3D reconstruction of histological sections: Application to mammary gland tissue. Microsc Res Tech 73:1019–1029
8. Ollion J, Cochennec J, Loll F, Escudé C, Boudier T (2013) TANGO: a generic tool for high-throughput 3D image analysis for studying nuclear organization. Bioinformatics 29:1840–1841
9. Pelleg D, Moore AW (2000) X-means: extending K-means with efficient estimation of the number of clusters. In: Proceedings of the Seventeenth International Conference on Machine Learning. Morgan Kaufmann Publishers Inc, pp 727–734